European Journal of Pharmaceutics and Biopharmaceutics 201 (2024) 114349

Contents lists available at ScienceDirect

European Journal of Pharmaceutics and Biopharmaceutics

journal homepage: www.elsevier.com/locate/ejpb

Research paper

# Amine-functionalized mesoporous silica nanoparticles decorated by silver nanoparticles for delivery of doxorubicin in breast and cervical cancer cells

Melika Ghobadi [a], Saeideh Salehi [b], Mohammad Taha Salmanifard Ardestani [c], Mohammad Mousavi-Khattat [d], Zahra Shakeran [d], Arezoo Khosravi [e], Marco Cordani [f,g,*], Ali Zarrabi [h,i,j,*]

[a] Department of Genetics, Department of Biology, Institute of Higher Education, Noor Danesh Maymeh, Isfahan, Iran
[b] Advanced Materials Research Center, Department of Materials Engineering, Najafabad Branch, Islamic Azad University, Najafabad, Iran
[c] School of Biology, Faculty of Science, University of Tehran, Tehran, Iran
[d] Department of Biotechnology, Faculty of Biological Science and Technology, University of Isfahan, Isfahan, Iran
[e] Department of Genetics and Bioengineering, Faculty of Engineering and Natural Sciences, Istanbul Okan University, Istanbul 34959, Türkiye
[f] Department of Biochemistry and Molecular Biology, Faculty of Biological Sciences, Complutense University of Madrid, 28040 Madrid, Spain
[g] Instituto de Investigaciones Sanitarias San Carlos (IdISSC), 28040 Madrid, Spain
[h] Department of Biomedical Engineering, Faculty of Engineering and Natural Sciences, Istinye University, Istanbul 34396, Türkiye
[i] Department of Research Analytics, Saveetha Dental College and Hospitals, Saveetha Institute of Medical and Technical Sciences, Saveetha University, Chennai 600 077, India
[j] Graduate School of Biotechnology and Bioengineering, Yuan Ze University, Taoyuan 320315, Taiwan

ARTICLE INFO

*Keywords:*
Mesoporous silica nanoparticles
Silver nanoparticles
Green synthesis
Doxorubicin
Breast cancer
Cervical cancer

ABSTRACT

Nanocarriers have demonstrated promising potential in the delivery of various anticancer drugs and in improving the efficiency of the treatment. In this study, silver nanoparticles (AgNPs) were green-synthesized using the extracts of different parts of the pomegranate plant, including the peel, flower petals, and calyx. To obtain the most efficient extract used for the green synthesis of AgNPs, all three types of synthesized nanoparticles were characterized. Then, (3-Aminopropyl) triethoxysilane-functionalized mesoporous silica nanoparticles (MSNs-APTES) decorated with AgNPs were fabricated via a one-pot green-synthesis method. AgNPs were directly coated on the surface of MSNs-APTES by adding pomegranate extract enriched with a source of reducing agent leading to converting the silver ion to AgNPs. The MSN-APTES-AgNPs (MSNs-AgNPs) have been thoroughly characterized using nanoparticle characterization techniques. In addition, DNA cleavage and hemolysis activities of the synthesized nanoparticles were analyzed, confirming the biocompatibility of synthesized nanoparticles. The Doxorubicin (DOX, as a breast/cervical anti-cancer drug) loading (42.8%) and release profiles were investigated via UV–visible spectroscopy. The fibroblast, breast cancer, and cervical cancer cells' viability against DOX-loaded nanoparticles were also studied. The results of this high drug loading, uniform shape, and small functionalized nanoparticles demonstrated its great potential for breast and cervical cancer management.

## 1. Introduction

Cancer, a disease characterized by uncontrolled cell growth, continues to be a significant health concern, accounting for more than 10 million new cases globally each year [1,2]. Among the myriad types of cancers, breast and cervical cancers are the leading causes of cancer-related death among women in developed countries [3,4]. In 2020 alone, breast cancer accounted for 2.30 million cases and 685,000 deaths, while approximately 570,000 cases of cervical cancer were estimated in 2018, leading to the death of approximately 311,000 women [5,6]. Current cancer treatment ranges from surgical intervention to chemotherapy, radiation therapy, or a combination thereof [2]. However, chemotherapy, a main treatment modality, has many disadvantages. These include poor absorption, the requirement of large dosages, unpleasant side effects, low therapeutic indices, the potential for the development of multiple drug resistance, and a lack of specific targeting [7]. Therefore, innovative drug delivery systems, such as nanocarriers including copolymers, micelles, hydrogels, dendrimers, metal

* Corresponding authors.
*E-mail addresses:* mcordani@ucm.es (M. Cordani), ali.zarrabi@istinye.edu.tr (A. Zarrabi).

https://doi.org/10.1016/j.ejpb.2024.114349
Received 15 February 2024; Received in revised form 18 May 2024; Accepted 4 June 2024
Available online 5 June 2024

nanoparticles, and mesoporous silica nanoparticles (MSNs) are being explored for targeted chemotherapeutic interventions, with the potential to improve the pharmacological profile of existing drugs [8,9]. In recent years, mesoporous materials including mesoporous carbon, mesoporous polydopamine, mesoporous silica, etc. have been widely developed to treat various types of tumors [10]. MSNs, known for their multiple applications in catalysis, nanomedicine, sensors, bioceramics, and drug delivery, are intriguing nanostructures [11]. Furthermore, MSNs were developed for nanodynamic therapy-related theranostics and multimodal synergistic therapy as well as they were promised candidates for photoactivated cancer therapy [12,13]. The unique attributes of these silica nanoparticles, including their controlled pore size, reduced drug toxicity, controllable drug release, high biodegradability, and large surface area, make them highly suitable as nanocarriers [14]. The fabrication of functionalized mesoporous silica materials provides a host framework for various drugs [15]. Furthermore, functionalizing the silica matrix with various organic moieties allows for higher loading capabilities and slower release rates [16,17]. This has been leveraged for the delivery of anticancer drugs for breast and cervical cancers [18,19].

Among metallic nanoparticles, silver nanoparticles (AgNPs) hold unique promise due to their diverse physical, chemical, and biomedical properties and have been employed in areas such as catalysts, adsorbents, antimicrobials, drug delivery, and fertilizers [20]. AgNPs can be synthesized through different methods, including physical, chemical, and green synthesis approaches [21–23]. Of these, the green synthesis method stands out due to its cost-effectiveness, environmental friendliness, and reduced toxicity [24–26].

Various species of plants, such as Punica granatum L., are efficient in converting silver ions to AgNPs due to their inherent reducing and stabilizing properties [27,28]. Compounds from this plant, abundant in many antioxidant components, have been reported to display potent cytotoxic activity against breast and cervical cancer cell lines, suggesting that green synthesized AgNPs coated with pomegranate extract could serve as a potential anticancer agent [27,29,30].

Different anticancer drugs, such as methotrexate, paclitaxel, tamoxifen, and doxorubicin, are used for the treatment of breast and cervical cancer [31–34]. Doxorubicin (DOX), an anthracycline glycoside antibiotic, has shown promising effects against various types of cancers including lung, cervical, ovarian, and breast tumors [35]. DOX, upon passive diffusion through the cell membrane, is converted into a semiquinone that generates reactive oxygen species (ROS), inducing DNA damage and energetic stress [36].

Various nano-sized delivery systems for DOX have been developed and approved for cancer treatment [34,37]. Recent advancements in material sciences and nanotechnology have improved DOX delivery through various nanostructures, which represent a promising strategy for more effective and feasible cancer treatment [38,39]. Notably, binary nanocarriers including MSNs coated with AgNPs have been developed to achieve high drug-loading ability [40]. Zhang et al. (2020) developed mesoporous silica-coated silver nano-frames as vehicles for multimodality therapy for the effective delivery of glucose oxidase and tirapazamine [38]. In another report, silver nanoparticle-gated MSNs were applied for glutathione delivery with controlled release in cancer environments [40]. He et al. (2022) comprehensively investigated the fabrication of MSNs-Ag nanoparticles for combination Therapies for cancer and infection. Therefore, they first described various structures such as star-shaped structures, core–shell structures, and Janus structure MSNs-Ag nanoparticles, and then highlighted Ag-MSNs as a multifunctional nanoplatform to surface-enhanced Raman scattering-based detection, non-photo-based cancer theranostics and photo-based cancer theranostics [41].

This study aims to improve the delivery of anticancer agents by synthesizing MSNs and AgNPs from different materials. Firstly, AgNPs were synthesized using a green synthesis method that employed different parts of the pomegranate plant. Concurrently, MSNs were synthesized using different precursors and then modified with (3-Aminopropyl) triethoxysilane (APTES). The presence of CTAB as a template is necessary for the formation of micelle units and creates mesopores in silica nanoparticles. The Pluronic™ F-127 co-polymer was interpreted to have enabled a decrease in the size of the nanoparticles below 100 nm [42]. APTES has three functional reactive ethoxy groups and one amine group, used to introduce positive charges onto the negatively charged SiO2 surface. The resulting structure can bind to silver nanoparticles [43,44]. Silver ions were subsequently attached to the functionalized surfaces of MSNs and reduced to silver nanoparticles using the green synthesis method with the calyx of the pomegranate plant. Each step was carefully characterized to confirm the successful synthesis process. The synthesis method was then optimized for the delivery of DOX, a drug widely used for the treatment of breast and cervical cancers. Lastly, we conducted a panel of different in vitro assays, such as the hemolysis evaluation, DNA cleavage of human red blood cells, and the cell viability studies of MCF-7, Hela, and L929 cells using different concentrations of DOX-loaded binary nanoparticles. The results were compared to free DOX and free nanoparticles. Our findings indicated a remarkable induction in DNA cleavage, inhibition in hemolytic activity, and cancer cell proliferation, thus highlighting the potential of these novel nanocarriers systems in enhancing the efficacy of cancer treatment.

## 2. Materials and Method

### 2.1. Materials

Tetraethyl orthosilicate (TEOS, ≥99 %), Tetramethyl orthosilicate (TMOS, ≥99 %), Hexadecyltrimethyammonium bromide (CTAB, ≥99 %), sodium hydroxide (NaOH, ≥98 %), Pluronic™ F-127 (Quality Level: 200), hydrochloric acid (HCl, 37 %), ethanol (EtOH, 96 %), methanol (MeOH, ≥99.9%), 3-triethoxysilylpropylamine (APTES, 99 %), Dimethyl Sulfoxide (DMSO) were purchase from Sigma-Aldrich (Germany). Dulbecco's modified Eagle's medium (DMEM), fetal bovine serum (FBS), Penicillin–streptomycin (10,000 U ml/ml), trypsin-EDTA (0.25 %) was obtained from GIBCO® (Thermo Fisher Scientific, MA, USA), Doxorubicin was purchased from Actoverco pharmaceutical company (Iran).

### 2.2. Nanoparticle synthesis

#### 2.2.1. Preparation of plant extracts for green synthesize of AgNPs

Fruits of Punica granatum L. were harvested from the University of Isfahan's greenhouse, in Isfahan, Iran. Selected parts of the pomegranate fruit, including the peel, flower petals, and calyx were isolated, dried, and then ground into powder. For each extract, 1.50 gr of the respective powders were combined with 30 ml of distilled water. The mixture was heated to 80 °C and stirred for 15 min. Finally, each mixture was filtered using filter paper (Whatman No. 1), and the pH was adjusted to 8.5 individually [45].

#### 2.2.2. Antioxidant activity of plant extracts

The antioxidant properties of the peel, flower petals, and calyx extract were determined using the 1,1-diphenyl 2-picrylhydrazyl (DPPH) free radical scavenging assay. To this end, a stock solution of DPPH (0.039 mg/ml), dissolved in methanol, was prepared. Next, 2 ml of the DPPH solution was mixed with 1 ml of plant extract samples at different concentrations (0.2–4 μg/ml) and then incubated in the dark for 30 min. A blank sample was prepared by substituting 1 ml of distilled water for the plant extract. Absorbance was measured at 517 nm, indicating the remaining DPPH concentration. The percentage of DPPH radical scavenged was calculated using Equation (1) [46]:

$$\text{DPPH scavenging effect}\,(\%) = \frac{(\text{Blank absorbance} - \text{Sample absorbance})}{\text{Blank absorbance}} \times 100 \quad (1)$$

### 2.2.3. Green synthesis of silver nanoparticles

The green synthesis of AgNPs was achieved using the peel, flower petals, and calyx extracts of the pomegranate plant. For each reaction, 0.34 g of silver nitrate was dissolved in distilled water to yield a 4.0 mM AgNO3 solution, which was then heated to 80 °C under continuous stirring. Subsequently, 10 ml of each plant extract was added to three separate batches, with stirring maintained at 80 °C for 24 h. The mixtures were then centrifuged at 14,000 RPM for 15 min and the resulting pellets were washed with distilled water.

### 2.2.4. Synthesis of bare MSNs

Bare MSNs were synthesized employing a modified sol–gel method [47]. Briefly, 120 ml of deionized water was mixed with 720 µl of 2 M NaOH, followed by the addition of 250 mg of CTAB and 200 mg of Pluronic™ F-127. The solution was heated to 80 °C and stirred for 1 h. Then, 1.50 ml of TEOS was introduced, and the ensuing white suspension was further stirred for 2 h at 80 °C. The same procedure was carried out with 400 µl of TMOS substituting for TEOS. Finally, an acidic methanol solution was used to remove the CTAB mesoporous templates at 60 °C for 24 h. The resulting MSNs pellets were washed three times with ethanol and water, followed by centrifugation.

### 2.2.5. Msns functionalization with APTES

Surface functionalization of MSNs with APTES was performed using grafting techniques. Initially, 100 mg of MSNs were dispersed in 70 ml of ethanol and subjected to sonication. This was followed by the addition of 3 ml of water and 1.50 ml of glacial acetic acid while maintaining constant stirring. Then, 100 µl of APTES was incrementally introduced into the reaction mixture, and this configuration was stirred for 24 h. The resulting suspension was then thoroughly washed with ethanol and water.

### 2.2.6. Formation of AgNPs on the surface of amine-functionalized MSNs

The APTES-functionalized MSNs, synthesized following a slightly adapted Cai reaction, were subsequently coated with AgNPs [44,48]. This process involved the preparation of three solutions. **Solution A** comprised 100 mg of APTES-functionalized MSNs dispersed in 150 ml of distilled water, heated to 80 °C under stirring conditions; **solution B** was prepared by dissolving 100 mg of AgNO3 in 50 ml of distilled water, again under stirring and heating at 80 °C; **solution C** consisted of 500 mg of pomegranate calyx dispersed in 10 ml of distilled water, heated and stirred at 80 °C. The mixture was then filtered, and the pH of resulting extract was adjusted. After heating and stirring suspension A for 30 min, solution B was incrementally added to suspension A, and the combined mixture was heated at 80 °C for 1 h while stirring vigorously. Then, 4 ml of plant extract from suspension C was introduced, and heating and stirring were continued for another 24 h. Finally, the suspension was washed with distilled water three times.

### 2.2.7. Characterization

The morphology, size, and nanostructures of AgNPs, MSNs, and MSNs-AgNPs were examined using a Field Emission Scanning Electron Microscope (FEI-SEM; QUANTA FEG-450, FEI Company, USA). The analysis was conducted at an accelerating voltage of approximately 10 kV and a working distance of roughly 5 mm. Moreover, MSNs-AgNPs were analyzed using EDX and elemental mapping. Furthermore, the morphological features of MSNs, MSNs-APTES, and MSNs-AgNPs were investigated using Transmission Electron Microscopy (TEM) on a Carl Zeiss-EM10C (Germany), set at an accelerating voltage of 100 kV. The formation of AgNPs using three different extracts from the pomegranate plants (peel, flower petals, and calyx extract) was monitored separately via UV–vis spectroscopy between 300 to 600 nm.

Fourier-transform infrared (ATR-FTIR) spectroscopy (Bruker model, TENSOR 37, Germany) was employed to analyze the deposition of phytochemical compounds on the surfaces of the green synthesized AgNPs. The presence of silver in the green synthesized nanoparticles, derived from peel, flower petals, and calyx extracts of the pomegranate plant was confirmed using a D8 Advanced X-ray Diffractometer equipped with a Cu Kα source (Bruker, Germany).

The hydrodynamic diameter, size distribution and stability of nanoparticles were assessed through Differential light scattering (DLS) and zeta potential (ζ- potential) analysis, using a Malvern Zetasizer Nano ZS (Malvern Instruments, Worcestershire, UK). The material refractive index (RI) was set to 1.54, and the water dispersant refractive index was 1.33, with measurement taken at 25 °C, and a pH range of 6.8–7.0.

To measure the quantity of nanosilver attached to the functionalized silica nanoparticles, a suspension containing 300 mg of the synthesized nanoparticles was centrifuged. The resulting pellet was thoroughly washed with water to collect the free nanoparticles. Then, the free nanoparticles present in the suspension and the bonded nanoparticles in the precipitated sample were quantified using inductively coupled plasma optical emission spectroscopy (ICP-OES) (VISTA-PRO, Varian, Palo Alto, CA).

## 2.3. Dox loading and release

DOX-hydrochloride was combined with MSNs-AgNPs in varying ratios of DOX: NPs (1:10, 1:5, 1:2, and 1:1 w/w). Thus, different quantities of MSNs-AgNPs (20, 10, 4, and 2 mg) were dispersed in 1 ml of deionized water. Simultaneously, 2 mg of DOX- hydrochloride was dissolved in deionized water (1 ml), followed by the gradual addition of the MSNs-AgNPs suspension under gentle stirring at room temperature for 24 h. The suspension was then centrifuged to obtain the DOX-leaded MSNs-AgNPs and washed with deionized water to remove any free DOX- hydrochloride in the suspension. The supernatants from each washing step were collected for UV–Visible detection (480 nm) to calculate the DOX-hydrochloride loading efficiency (LE%) and loading capacity (LC%). For quantitative analysis, a standard calibration curve was plotted using different concentrations of DOX- hydrochloride, ranging from 0.031 to 0.5 mg/ml. The absorbance of the supernatant was used for the calculation of loading content, which was measured in triplicate, using Equation (2):

$$\text{Loading content}\,(\text{LC})\,\% = \frac{\text{amount of DOX loaded in MSNs} - \text{AgNPs}}{\text{total amount of MSNs} - \text{AgNPs}} \times 100 \quad (2)$$

The availability of DOX in the MSNs-AgNPs was determined by the amount of the loaded DOX under encapsulation efficiency (EE) and it was calculated by Equation (3):

$$\text{Encapsulation efficiency}\,(\text{EE})\,\% = \frac{\text{amount of DOX loaded in MSNs} - \text{AgNPs}}{\text{initial amount of DOX}} \times 100 \quad (3)$$

The DOX release profile from MSNs-AgNPs was studied by dispersing the drug-loaded nanocarriers in a PBS buffer, replicating the microenvironment of cancer cells (pH = 6.8). The suspensions were agitated at predetermined intervals (0.5–96 h) at 37 °C and the suspensions were centrifuged at each time, the supernatant was collected, and the release medium was replenished with an equal volume of fresh buffer. The DOX content of the supernatant was quantified each time using a microplate reader (Cat# 800TS, Biotek, USA), and the amount of released DOX was determined using the calibration curve. The release mechanism and kinetics of the DOX release were verified by analyzing the data against

several kinetic models, including Korsmeyer Peppas, Hixon-Crowell, zero order, first order, and Higuchi models. The prediction models were developed using linear regression equations, and the model with the highest $R^2$ value was selected to calculate the release kinetics of each drug.

### 2.4. DNA cleavage

The DNA cleavage capability of the synthesized nanoparticles, including green-synthesized silver nanoparticles using calyx extract, MSNs-APTES, and MSNs-AgNPs, was determined via agarose gel electr ophoresis. Peripheral blood DNA was extracted using phenol–chloroform methods [49]. Subsequently, each nanoparticle sample (5 µl, 10 mg/ml) was added to 5 µl of extracted DNA and incubated for 120 min. This was followed by treatment with a loading dye and electrophoresis on an agarose gel at 70 V for 30 min. Untreated genomic DNA served as the negative control, and the gel was inspected under UV light [46].

### 2.5. Hemolysis assay

The biocompatibility of the synthesized samples, including MSNs, AgNPs (green synthesized by calyx extract), MSNs-AgNPs, MSNs- DOX, MSN −AgNPs-DOX, and DOX, with human red blood cells was evaluated using a hemolysis assay. Firstly, 1 ml of human blood was centrifuged to isolate the erythrocytes, which were then diluted threefold with phosphate-buffered saline. Various concentrations of each sample were combined with the erythrocyte suspension, adjusting the final concentration of the sample solution in the range of 2 mg/ml to 10 mg/ml. The suspension was subsequently incubated at 35 °C for 1 h and centrifuged to collect the supernatant, which was dispensed into 96-well plates. Hemoglobin release was assessed by recording the absorbance at 540 nm. Water and DMSO served as positive and negative control, respectively. The percentage of hemolysis was calculated using Equation (4) [50]:

$$\text{Hemolysis}\,(\%) = \frac{(\text{Sample absorbance} - \text{Negative Control absorbance})}{\text{Positive Control absorbance} - \text{Negative Control absorbance}} \times 100 \quad (4)$$

### 2.6. Cell cytotoxicity

The cytotoxic effect of MSNs, MSN-AgNPs, AgNPs, MSN-AgNPs-DOX, free DOX, and MSN-DOX was assessed utilizing the MTT assay on MCF-7 cells (ATCC® number HTB-22™) and Hela cells (ATCC® Number: CCL-2™), which are representative of breast and cervical cancer respectively. Additionally, the viability of L929 cells (ATCC® number CCL-1™), which are derived from mouse fibroblast cells, was evaluated after exposure to the various synthesized samples using the MTT assay. All cells were purchased from the Isfahan University of Medical Sciences.

The fifth cell passage was cultured in DMEM supplemented with 10 % fetal bovine serum (FBS) and 1 % penicillin/streptomycin in a cell culture flask. Similar experiments were conducted for L929 cells, where RPMI media was replaced with DMEM media.

Cells were seeded in a 96-well cell plate at a density of $4 \times 10^4$ cells per well and allowed to adhere to the well bottom for approximately 12 h. Subsequently, the cells were then exposed to a range of concentrations of the synthesized samples, adjusting the final concentration to 0.01, 0.10, 1, 10, and 100 µg/ml, equivalent to the concentration employed for free DOX. Untreated cells served as the control group.

Post 24 h incubation, 20 µl of MTT solution (5 mg/ml) was added to each well and further incubated for 3 h. Thereafter, 100 µl of DMSO was added to each well to dissolve the resulting formazan crystals, followed by a 20-minute incubation. The MTT absorbance was then recorded at 570 nm using a microplate reader (Cat# 800TS, Biotek, USA). The medium inhibitory concentration (IC50) was calculated for the samples. The synergistic effect of combining the chemotherapy and the presence of AgNP therapy can be assessed by calculating the combination index (CI) [51]. All experiments were repeated in triplicate and statistical analysis was performed using the post hoc Duncan's comparison of mean scores, considering a significance level of $P < 0.05$.

## 3. Results

### 3.1. Physicochemical properties of the nanoparticles

The physicochemical properties of the green synthesized AgNPs, MSNs, and amine-functionalized MSNs were meticulously assessed. Morphology, size, structure, and surface characteristics were analyzed using SEM.

As shown in Fig. 1, the SEM analysis of green synthesized AgNPs using peel, flower petals, and calyx extracts of pomegranate plant revealed spherical, isotropic nanoparticles. The sizes were approximately 18.2 ± 0.7 nm, 15.0 ± 0.6 nm, and 13.7 ± 0.4 nm, respectively. A transition in sample color from light yellow to dark red was observed during the green synthesis process, indicative of successful nanoparticle synthesis. The UV–vis spectroscopic profiles of the green-synthesized AgNPs using the three above-mentioned extracts and AgNO3 were recorded at the 300 to 600 nm range. The maximum absorption wavelength for AgNPs was observed at 425 nm, with an increasing absorbance pattern for each sample, reflecting the reduction of silver ions to nanoparticles. Notably, nanoparticles synthesized using calyx extract displayed higher absorption intensity at this wavelength (Fig. 2a). ATR-FTIR spectra of green synthesized AgNPs, using peel, flower petals, and calyx extracts from the pomegranate plant, were generated to validate the phytochemical coating of the nanoparticles during the synthesis process (Fig. 2b). The similarity of the FTIR spectrum trends between the extract alone and the extract decorated the surface of silver nanoparticles confirmed the claim of the coating of silver nanoparticles by the extract. The presence of absorption peaks at 3339 $cm^{-1}$, 2130 $cm^{-1}$, and 1637 $cm^{-1}$ corresponded to phenolic compounds, C–H stretching bonds, and carbonyl groups, respectively. The XRD spectra were utilized to ascertain the Ag content in the green-synthesized nanoparticles. The wide-angle XRD diffraction patterns of AgNPs, indicated peaks at 2θ values of 38°, 44°, 64°, and 77° corresponding to (111), (200). (220), and (311) crystalline planes of cubic Ag crystal, respectively. The XRD pattern at 2θ values degree, as shown in Fig. 2c-2e, confirmed the generation of silver nanoparticles by the extracts. Moreover, the intensity of the XRD spectrum for the synthesis of silver nanoparticles using calyx extract was notably higher than those using other extracts.

The antioxidant activity of the green-synthesized AgNPs was also evaluated. The results revealed a more potent inhibitory activity for the calyx extract compared to the peel and flower petals of the pomegranate plant (Fig. 3). Based on these findings, the calyx extract was selected for subsequent experiments, given its superior physicochemical properties compared to the other extracts.

In this study, the binary nanosystem of MSNs coated with AgNPs has been developed to achieve high drug-loading capacity. Therefore, the synthesis and characterization of MSNs and coated MSNs were analyzed. SEM analysis of MSNs synthesized using TEOS and TMOS revealed nanoparticles exhibiting spherical and uniform structures. The average size of the MSNs synthesized by TEOS and TMOS was approximately

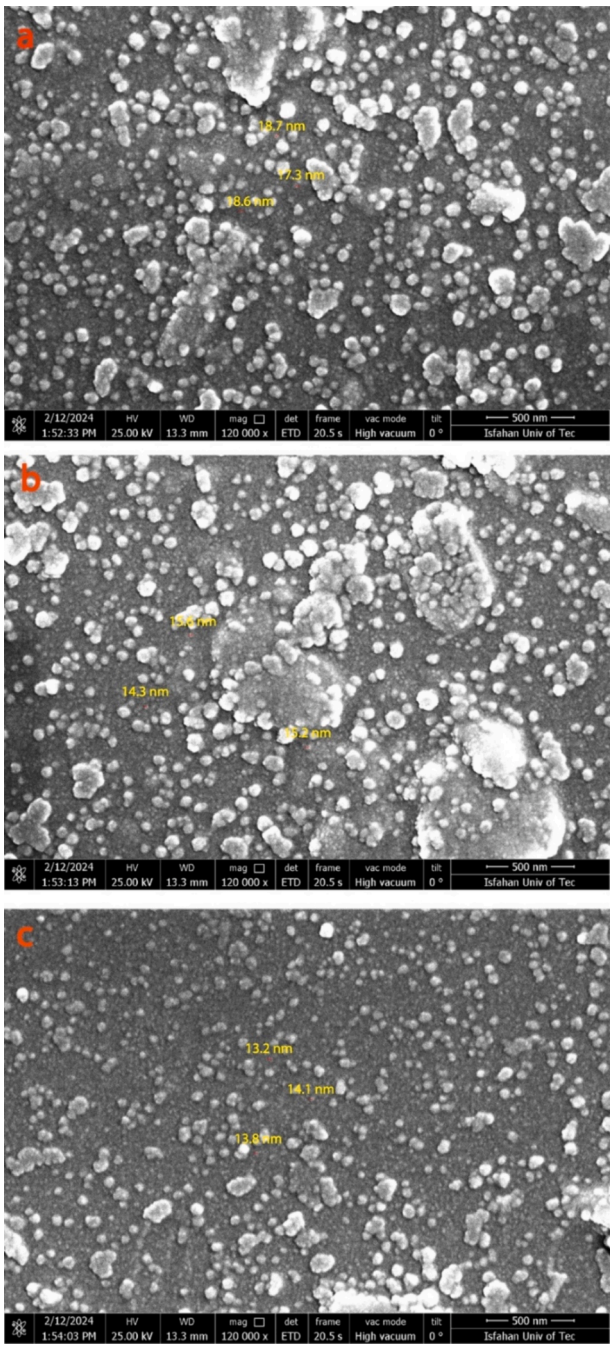


**Fig. 1.** SEM images of green synthesized AgNPs using a) peel, b) flower petals, and c) calyx extracts of pomegranate plant (Larger particles indicate the accumulation of silver nanoparticles, which is occurred by coating the sample with gold in FE-SEM analysis). (For interpretation of the references to color in this figure legend, the reader is referred to the web version of this article.)

62.08 ± 11.07 nm and 55.30 ± 5.47 nm, respectively. MSN modified with APTES, denoted as MSN-APTES, displayed almost isotropic, spherical morphology with an average size approximating 71.44 ± 7.05 nm. SEM analysis of MSNs coated with AgNPs disclosed uniformly dispersed, spherical functionalized MSNs with an average size of about 88.68 ± 3.85 nm (Fig. 4).

TEM images of the MSNs and MSNs-APTES confirmed the narrow size distribution of these nanoparticles and substantial their spherical shape with the hexagonal array. The average diameters of these nanoparticles were found to be 61.33 ± 4.04 and 66.33 ± 1.52 nm respectively. TEM analysis of MSNs-AgNPs provided insight into the diameter of spherical AgNPs on the surface of the amine-functionalized MSNs, revealing an average size of 4.33 ± 1.52 nm, indicative of a uniform dispersion (Fig. 4 **e–g**).

FE-SEM images, EDX, and elemental mapping of Ag nanoparticle-coated mesoporous silica nanoparticles are shown in Fig. 5 **a–f** and confirm the presence of Ag and silica as significant components.

The hydrodynamic diameter and size distribution of the MSNs, MSNs-APTEs, AgNPs, and MSNs-AgNPs were assessed using DLS. The results displayed a narrow size distribution for the samples, corroborating the data obtained from SEM data (Table 1).

Further insights into the stability and surface charge of the nanoparticles were obtained through zeta potential measurement, which hinges on the electrical double-layer formation around the charged nanoparticles (Table 1). The MSNs, after the removal of CTAB surfactants, exhibited a zeta potential value of approximately − 40.00 mV, suggesting a stable state optimal for modification by APTES, a source of positively charged amine groups. Following the APTES grafting process, the nanoparticles demonstrated a markedly positive surface charge, with a zeta potential of about + 32.50 mV. Interestingly, the zeta potential of the MSNs-AgNPs was measured to be approximately + 25.60 mV This deviation is attributed to the presence of AgNPs, which reacted with APTES on the surface of MSNs, thereby affecting the overall surface charge.

### 3.2. Quantifying coated AgNP content

The content of AgNPs, coated on the surface of functionalized MSNs, was determined to be approximately 9.80 wt%. This quantification was achieved through ICP methods, which assessed the presence of silver in the release medium. The successful coating of AgNPs on the surface of MSNs, employing the green-synthesized method, attests to the versatility of this approach for decorating amine-functionalized MSNs with AgNPs.

### 3.3. Dox loading and release assessment

DOX was combined with MSN-AgNPs at different ratios (1:10, 1:5, 1:2, and 1:1 w/w). After a 24-hour period, the LE% and LC% of the drug-nanoparticle samples were mathematically calculated using the UV–vis DOX standard curve. The results, as illustrated in Table 2, suggested that the LE% was comparable at the ratios of 1:5, 1:2, and 1:1, and these were lower than the 1:10 DOX: MSN-AgNPs ratio. However, the LC% at the ratios of 1:5, 1:2, and 1:1 was higher than the 1:10 ratio. If the amount of MSN-AgNPs is considered as a constant amount of 1 mg/ml, in this way, the ratio of DOX to MSN-AgNPs is 0.1:1, 0.2:1, 0.5:1, and 1:1 respectively. This result indicated that by increasing the amount of DOX, more drug is penetrated inside the pores or sited on the surface of the nanoparticle. The 1:1 ratio was selected for further experiments due to its superior loading capacity percentage. The cumulative drug release profile was analyzed under simulated cancer cells microenvironment conditions (pH = 6.8). The results indicated a slow release of DOX from the nanoparticles, as shown in Fig. 6. Table 3 presents the results of analyzing various kinetic models for the release profiles, demonstrating that the Higuchi model had the highest $R^2$ value for DOX release profiles.

### 3.4. DNA cleavage

The ability of the synthesized nanoparticles to cleave genomic DNA was assessed. In the design of drug delivery nanosystems, it is important that the system should not have side effects on normal cells. Therefore, preventing DNA cleavage of these cells is one of the main purposes in drug delivery systems. The results revealed that the DNA duplex exposed to AgNPs underwent significant cleavage. However, when the DNA was exposed to MSN-AgNPs, DNA fragmentation was notably reduced. The bond observed in the good region of the electrophoresis gel corresponds to the amine-functionalized silica nanoparticle sample. This outcome is

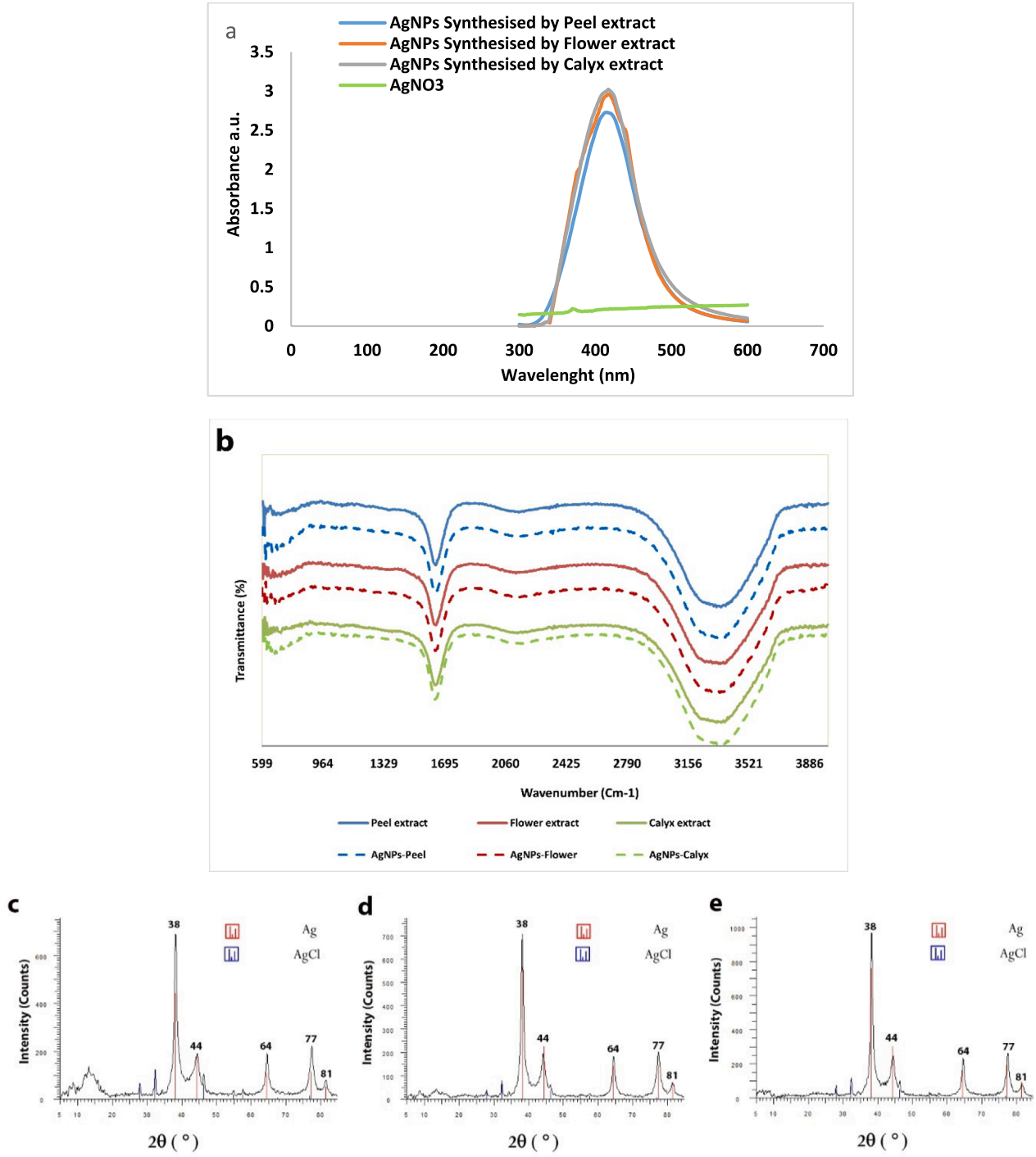


**Fig. 2.** Analysis of green-synthesized AgNPs using peel, flower petals, and calyx extracts of pomegranate plant by a) UV–vis spectroscopy of green-synthesized AgNPs by the extracts compared with AgNO3, b) ATR-FTIR spectrum of extracts (line) and biosynthesized AgNPs by the extracts (dash-dotted line), and c-e) The wide-angle X-Ray diffraction spectra of AgNPs, indicated peaks at 2θ values crystalline planes of face-centered cubic AgNPs. (For interpretation of the references to color in this figure legend, the reader is referred to the web version of this article.)

likely due to the presence of amino groups on the nanoparticle's surface (Fig. 7). These findings suggest that the functionalization of silica nanoparticles with amino groups can have a protective effect, potentially reducing genomic damage during treatment.

### 3.5. Hemolysis assay

The hemolytic activity of the synthesized nanoparticles was assessed at a wavelength of 540 nm. Our data demonstrated that the green-synthesized AgNPs induced a higher percentage of red blood cell hemolysis compared to other samples. Interestingly, this hemolytic activity decreased when silver nanoparticles were complexed with mesoporous silica nanoparticles. Furthermore, the encapsulation of doxorubicin within the MSNs and MSN-AgNPs complex resulted in a reduction of their hemolytic activity, particularly at higher concentrations (Fig. 8). These findings suggest the potential of MSNs and their complexes to reduce hemolytic side effects, enhancing the safety profile of anticancer treatments.

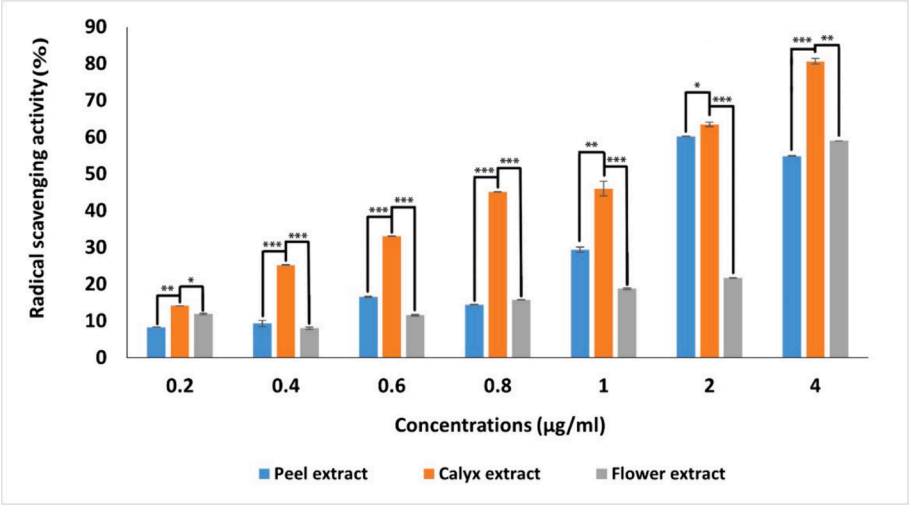


**Fig. 3.** The antioxidant activity of the green-synthesized AgNPs using three extracts. The plant extracts at different concentrations (0.2–4 µg/ml) and DPPH were mixed for 30 min, and absorbance was measured at 517 nm. The asterisk represents significant differences in mean values for each parameter using Duncan's test (* $P < 0.05$, ** $P < 0.01$, *** $P < 0.001$). (For interpretation of the references to color in this figure legend, the reader is referred to the web version of this article.)

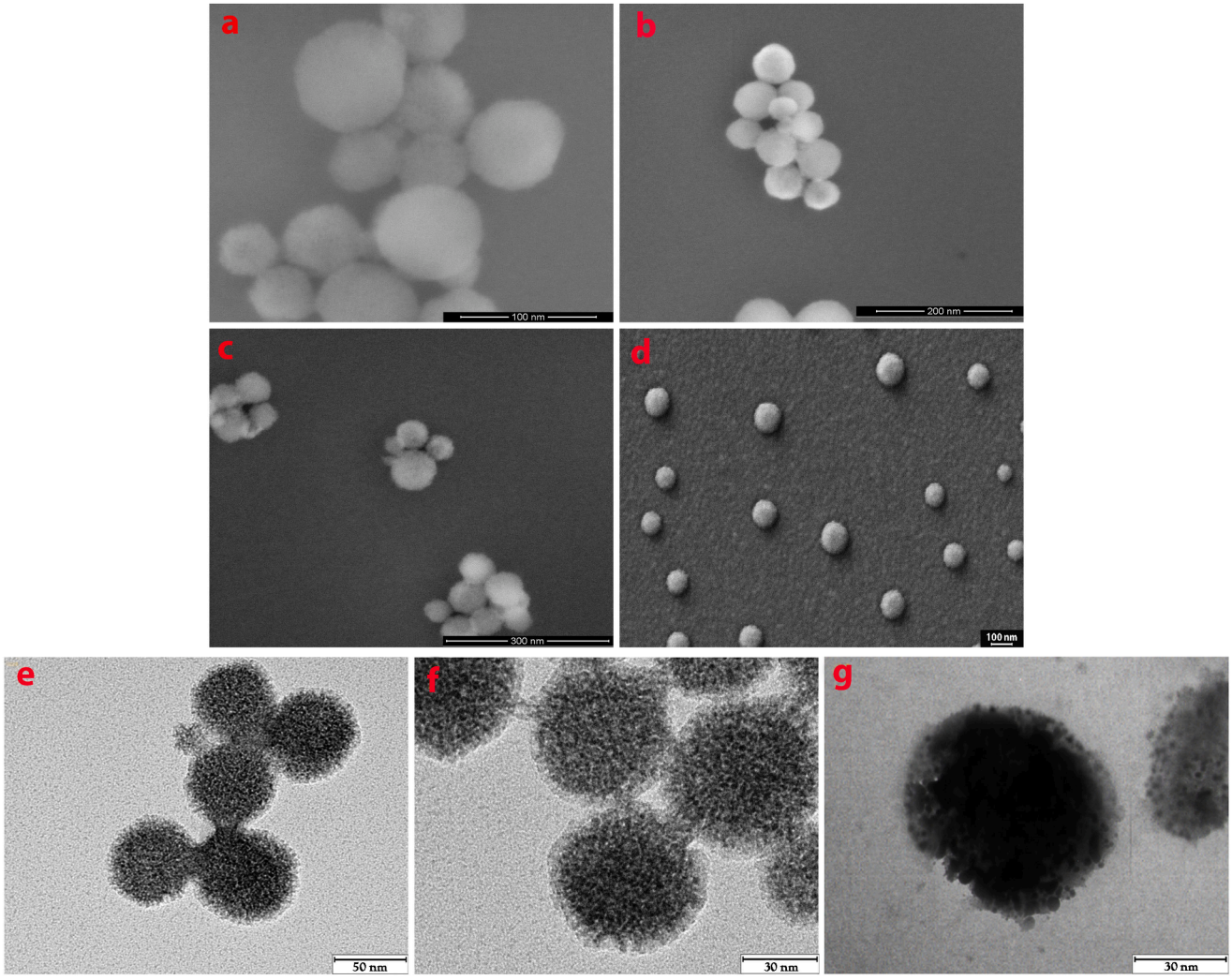


**Fig. 4.** A-b) sem images of mesoporous silica nanoparticle using tmos and teos as silica precursors for sol–gel synthesize of the nanoparticles respectively, c-d) SEM images of modified-MSNs include MSN-APTES and MSN-APTES-AgNPs respectively, e-g) TEM images of MSNs, MSN-APTES, and MSN-APTES-AgNPs respectively.

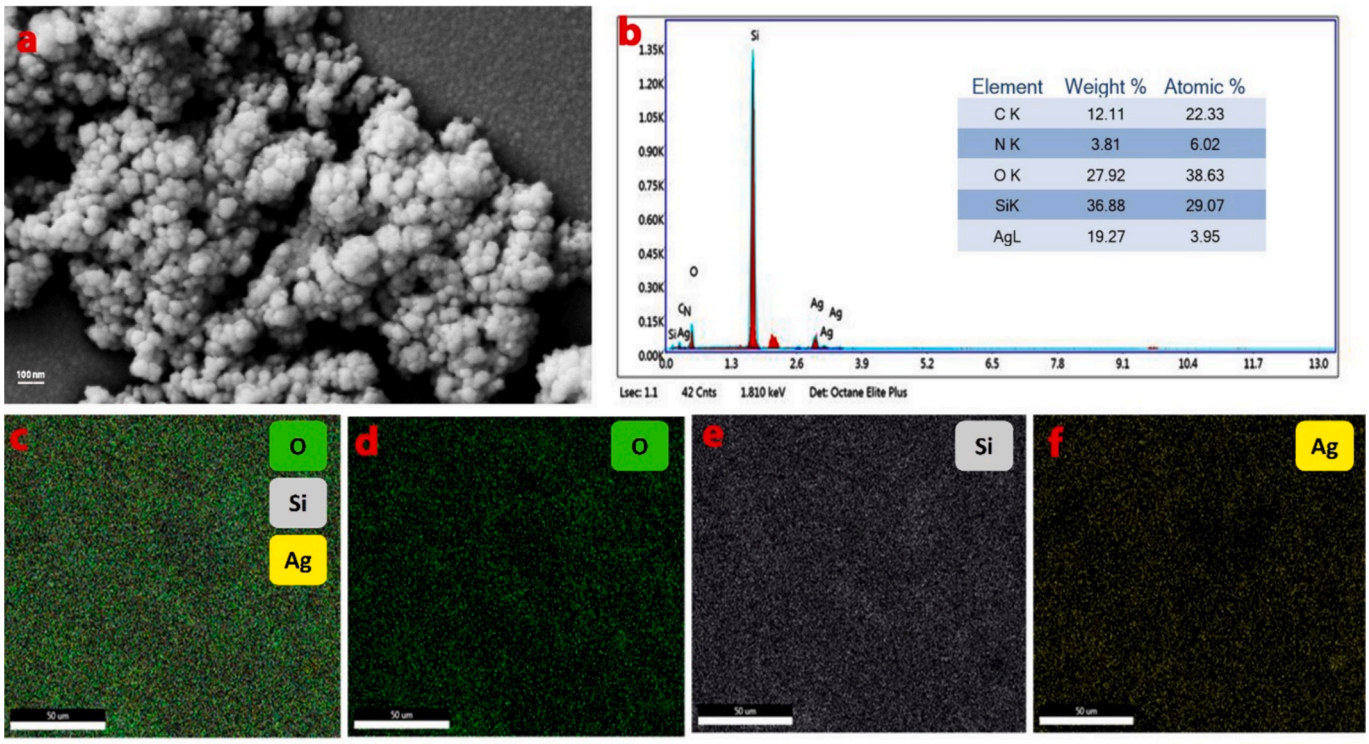


**Fig. 5.** FE-SEM images and EDX of Ag nanoparticles coated mesoporous silica nanoparticles (a), and (b) respectively. (c-f) shows the elemental mapping for Ag-coated MSNs.

**Table 1**
Characterization of physicochemical properties of MSNs, MSN-APTES, and MSN-APTES-AgNPs samples (hydrodynamic size, polydispersity index (PDI) and Zeta potential).

| No. | Sample | $D_H$ (nm) | PDI | Intercept | Zeta potential (mV) |
|---|---|---|---|---|---|
| 1 | MSNs | 78.90 ± 10.40 | 0.080 ± 0.001 | 0.95 ± 0.001 | −39.90 ± 0.50 |
| 2 | MSN-APTES | 89.40 ± 9.30 | 0.12 ± 0.001 | 0.91 ± 0.001 | +32.50 ± 0.40 |
| 3 | MSN-APTES-AgNPs | 98.50 ± 8.70 | 0.15 ± 0.001 | 0.96 ± 0.001 | +25.60 ± 0.60 |

**Table 2**
The Loading Efficiency (LE), Loading Capacity (LC), and Cumulative Release Percentage of the DOX using UV–vis spectroscopy.

| Number | Samples With Different Loading Ratios | LE% | LC% | Cumulative Release% |
|---|---|---|---|---|
| 1 | DOX: MSN-APTES-AgNPs (1:1) | 42.80 ± 0.10 | 42.80 ± 0.10 | 65.20 ± 0.001 |
| 2 | DOX: MSN-APTES-AgNPs (1:2) | 43.40 ± 0.25 | 21.70 ± 0.12 | – |
| 3 | DOX: MSN-APTES-AgNPs (1:5) | 43.93 ± 0.50 | 8.78 ± 0.10 | – |
| 4 | DOX: MSN-APTES-AgNPs (1:10) | 75.33 ± 0.38 | 7.53 ± 0.03 | – |

### 3.6. Cell cytotoxicity

The cytotoxicity of various samples, including MSNs, MSN-AgNPs, AgNPs, MSN-AgNPs-DOX, DOX, and MSN-DOX was evaluated in MCF-7, Hela, and L929 cell lines using the MTT assay. Initially, the cells were cultured in a flask and then seeded in a 96-well cell culture plate. Subsequently, they were treated with different concentrations of the aforementioned samples, with untreated cells serving as the control. After incubation, the cells were treated with an MTT solution, and the absorbance of the MTT product was measured at 570 nm.

The results for MCF-7 cell viability revealed that at a concentration of 100 μM MSN-AgNPs-DOX, the cell viability was approximately 30 %. In contrast, cell viability for free nanoparticles including MSNs, AgNPs, and MSN-AgNPs was approximately 100 %, 40 %, and 67 %, respectively.The Hela cell viability, after treatment with DOX-loaded MSN-AgNPs, was around 50 % at a concentration of 10 μM, indicating that half of the cells were non-viable.Interestingly, when L929 cells were treated with the lowest observed amount of MSN-AgNPs-DOX, cell viability was noted to be L929 74 % at a concentration of 100 μM. Upon treatment with a DOX concentration of 1 μM, the lowest viability percentage observed was 60 % for these cells (Fig. 9). Comparing the effect of MSNs-AgNPs-DOX on MCF-7 cells with L929 cells as the normal cells at a concentration of 100 μM clearly shows that the nanostructures-drug system has a significant effect on the survival of breast cancer cells, while it does not affect the viability of normal cells. Similar results were observed for the comparison of L929 cells and HeLa cells at concentrations of 1 and 10 μM. The IC50 was used for the calculation of the combination index (CI) and possible synergy (Table 4). As expected, compared with the group without AgNPs, the IC50 value of MSN-AgNPs-DOX rapidly reduced from 240.6 μM to 67.24 μM on the MCF7 cell line. Also, the IC50 value of MSN-AgNPs in the presence of DOX was lower than that of blank MSN-Ag (392.3). The CI analysis in this study for MCF7 was 0.451. Moreover, the IC50 of MSN-AgNPs-DOX, MSN-DOX, and MSN-AgNPs was 10.0, 235.8, and 20.7 on Hela cells, respectively. Therefore, the calculated CI value was 0.522. Consequently, the results demonstrate the synergistic effect of chemotherapy and the presence of AgNPs on both cell lines (CI $>$ 1, $=$1, or $<$ 1, indicates antagonistic, additive, or synergistic effects, respectively) [51]. These findings indicate that the coupling of AgNPs with MSNs and the subsequent loading of DOX significantly enhances cytotoxicity, shedding light on the potential of these substances for effective cancer treatment.

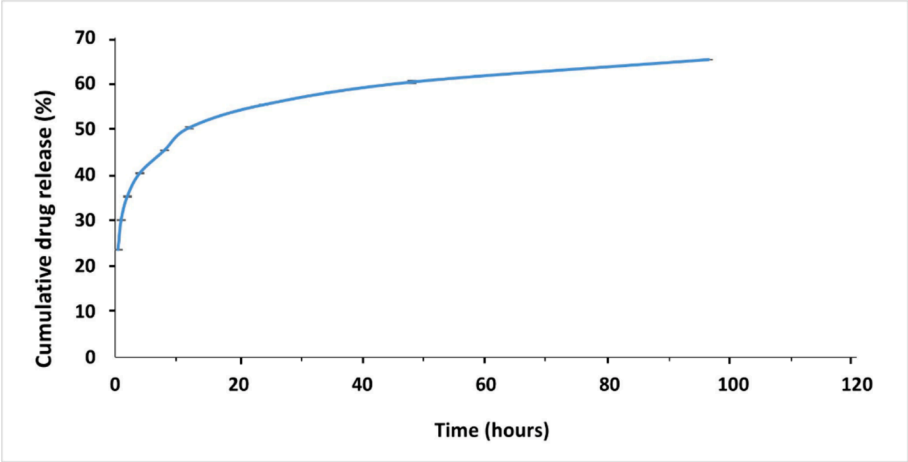


**Fig. 6.** Cumulative drug release profile of DOX under simulative cancer cells microenvironment (pH = 6.8) at 37 °C, over time in the buffer solution as release media measured by UV–vis absorbance at a wavelength of 485 nm.

**Table 3**
$R^2$ values for drug release kinetic models.

| Formulation/ Model | Korsmeyer-Peppas | Hixson | Zero Order | First Order | Higuchi |
|---|---|---|---|---|---|
| **DOX release** | $R^2 = 0.32$ | $R^2 = 0.68$ | $R^2 = 0.64$ | $R^2 = 0.71$ | $R^2 = 0.90$ |

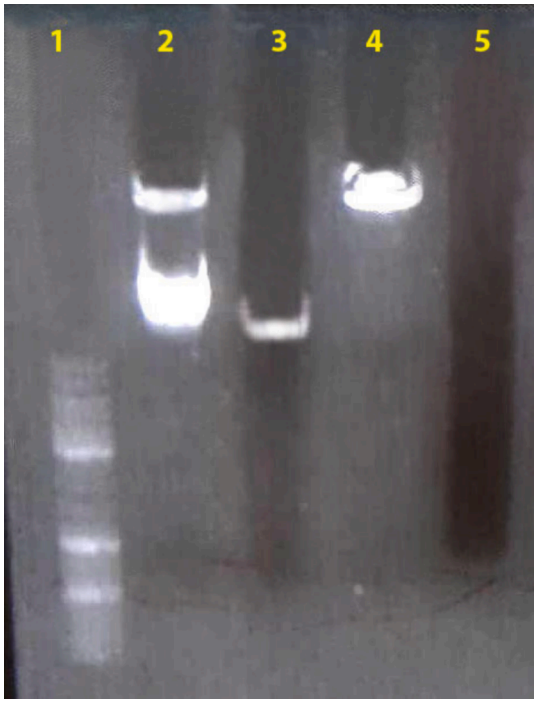


**Fig. 7.** DNA cleavage study of synthesized nanoparticles on genomic lymphocytes DNA using electrophoresis on an agarose gel at 70 V for 30 min., Lane 1: standard molecular weight DNA marker, lane 2: non-treated DNA as the negative control, lane 3: MSN-AgNPs, lane 4: MSN-APTES, lane 5: AgNPs.

$$CI = C1/Cf1 + C2/Cf2$$

$$CI = (MSN - APTES - AgNPs - DOX)/(MSN - APTES - DOX) + (MSN - APTES - Ag - DOX)/(MSN - APTES - AgNPs)$$

where Df1 is the dose of Drug-1 required to produce x percent effect alone and D1 is the dose of Drug 1 required to produce the same x percent effect in combination with Drug-2; similarly, Df2 is the dose of Drug2 required to produce x percent effect alone and D2 is the dose of Drug- required to produce the same x percent effect in combination with Drug-1 [52].

## 4. Discussion

Chemotherapy remains a prevalent treatment modality for cancer, although with significant limitations due to its non-selective action on cells, causing a range of side effects. Doxorubicin (DOX), a potent chemotherapeutic agent, has been widely employed in the management of multiple types of cancers, including advanced follicular lymphoma, multiple myeloma, hepatocellular carcinoma, clone cancers, carcinoma of the urinary bladder, breast cancer, and cervical cancer. However, its clinical application is often hampered by severe side effects, particularly nephrotoxicity and hepatotoxicity [53].

Nanomedicine, particularly the use of nanocarriers, offers novel opportunities for targeted delivery of chemotherapeutic agents, enhancing their efficacy while potentially mitigating side effects [54]. In this study, we utilized amine-functionalized MSN-AgNPs for the delivery of DOX. This novel approach demonstrated efficient cytotoxicity against breast cancer and cervical cancer cells. AgNPs were synthesized on the surface of MSN-APTES using an eco-friendly method involving the aqueous extract of a pomegranate plant Fu et al. (2023), evaluated the Pomegranate Peel Extract-Mediated Green Synthesis of AgNPs [55]. In other studies, the use of pomegranate peel extract for the green synthesis of AgNPs has been evaluated as a novel strategy to combat multi-drug resistant (MDR) bacteria [56–58]. Previous studies have reported that various parts of the pomegranate plant possess therapeutic potential against breast and cervical cancers [27,30,59].

SEM imaging showed that the green synthesized AgNPs, with a size of approximately 13 nm, exhibited uniform spherical morphology. Furthermore, the ATR-FTIR spectrum confirmed the presence of phenolic compounds and carbonyl groups on the surfaces of the nanoparticles, which are known to possess, anticancer properties and could reduce silver ions to silver nanoparticles [27,60].

Evaluation through UV–vis spectroscopy and XRD spectra revealed that the calyx extracts of the pomegranate plant produced a higher quantity of AgNPs with more potent antioxidant activity compared to the peel and flower petals extracts. This finding aligns with the investigation of Amri et al. (2017) who reported higher antioxidant activity in specific parts of two pomegranate plant varieties [61]. SEM analysis of MSNs synthesized by TEOS and TMOS showed a spherical and uniform

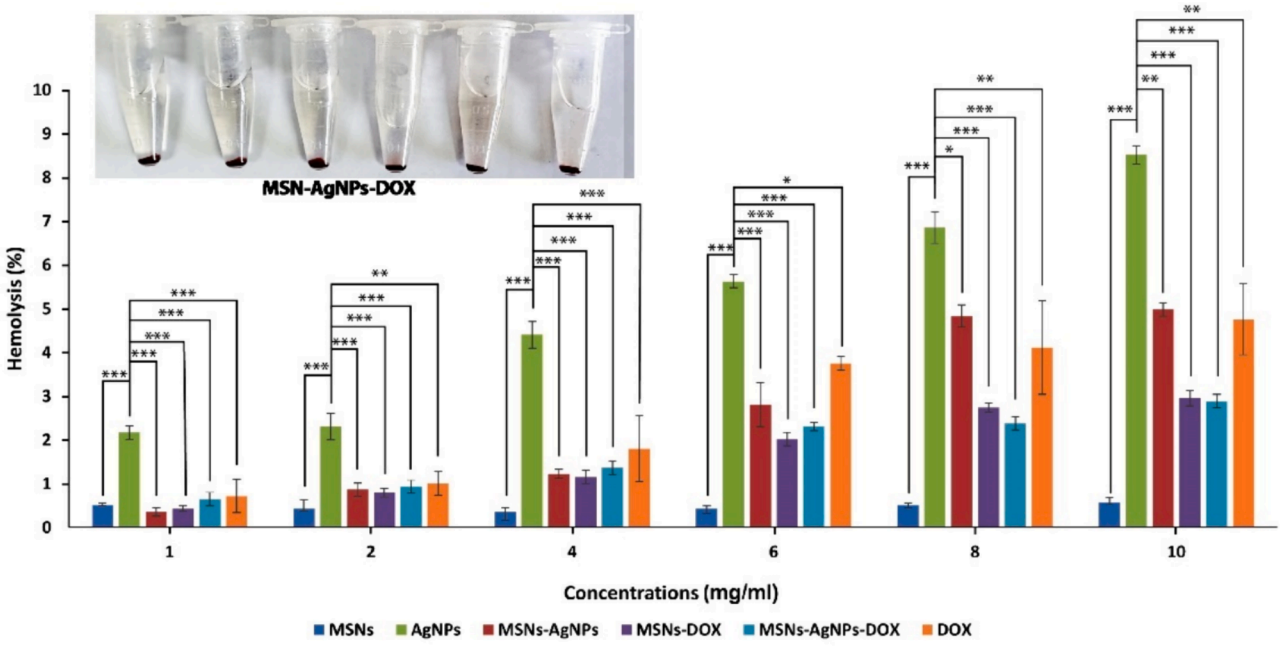


**Fig. 8.** The hemolytic activity of synthesized nanoparticles including MSNs, AgNPs, MSNs-AgNPs, and DOX-loaded nanoparticles compared with free DOX. Different concentrations of each sample were mixed with erythrocyte suspension incubated at 35 °C for 1 h and Absorbance was measured at 540 nm. The photo of the hemolysis analysis of the MSN-AgNPs-DOX sample is shown at the top of the graph. In this photo, it is clear that in the samples with a concentration of 1 to 6 (mg/ml), the supernatant in each vial is clear, and very little hemolysis has occurred. Also, in the samples with a concentration of 8 and 10 (mg/ml), a slight hemolysis can be observed. The asterisk represents significant differences in mean values for each parameter using Duncan's test (* $P < 0.05$, ** $P < 0.01$, *** $P < 0.001$).

structure, suggesting the suitability of both silica precursors for nanoparticle synthesis. This is supported by the findings of Sun et al. (2017), who reported that the synthesis of amine-functionalized silica nanoparticles was not influenced by the type of silane and amino silane molecules used [62]. Moreover, the functionalization of MSNs with APTES via the grafting method resulted in a positive zeta potential, indicating their stability [42,63]. Amine-functionalized MSNs were coated with AgNPs using AgNO3 and pomegranate plant calyx extract for the green-synthesize of AgNPs on the surface of MSNs-APTES. Silver ions can be readily embedded within the APTES structure on the surface of MSNs, followed by reduction with plant extract to form AgNPs. EDAX and elemental mapping confirm the presence of Ag-inserted MSNs. The presence of AgNPs-decorated MSN-APTES was confirmed using the ICP method. Tian et al. (2014), described a one-pot synthesis method for MSNs coated with silver nanoparticles using N-(aminoethyl)-aminopropyl trimethoxysilane (TSD) as an aminosilane molecule, covalently attached on the surface of MSNs. Silvers were reduced on the MSN-TSD surface using formalin [44]. Li et al. (2022) developed the formation of rod-like silver nanoparticles in the internal porous channels of mesoporous silica nanoparticles (MSN) via in-situ reduction of silver ions ($Ag^{+}$) by n-butylamine and the rod shape of the Ag nanoparticles obtained with an average length of about 250 nm and width of around 110 nm [64]. In this study, silver ions were reduced on the MSN-APTES surface by calyx extract and the average size of the complex was about 88.68 ± 3.85 nm. Pomegranate compounds exhibit potent cytotoxic activity in human breast and cervical cancer cell lines [29]. The loading of DOX onto MSN-AgNPs at different drug: nanoparticles ratios was investigated. The highest loading efficiency percentage was associated with the drug: nanoparticles ratio of 1: 10, while the highest loading capacity percentage was related to the ratio of 1: 1. The results indicated that the nanoparticles were saturated with DOX, which could be achieved by loading the drug into the porosity and onto the MSN-AgNPs surface. In addition, the cumulative drug release profile showed that the release of DOX from the nanoparticles was gradual, a desirable characteristic for drug delivery systems targeting cancer cells. Tang et al. (2012) developed a novel aptamer-targeted drug delivery system based on MSN-DOX and found that the slow release of DOX from the nanoparticles occurred with or without the presence of laser radiation with no significant difference[65]. Cumulative release results showed that DOX was slow to release and followed the Higuchi model. These models convey the drug release from a permeable matrix resembling this carrier. In the present system, MSNs form a porous structure, which provides a good loading of DOX, followed by release, and makes the release thermodynamically stable [45].

After characterizing our nanoformulation we moved to evaluate some biological effects, that could be exploited in the context of anticancer therapy. DNA cleavage assay demonstrated that the rate of DNA cleavage was reduced when AgNPs were coated with the functionalized MSNs, compared to the use of free AgNPs. These observations suggest that when silica nanoparticles are functionalized with amino groups, they could have a protective effect and reduce cytotoxic side effects during chemotherapy treatment. This corroborates their potential use as safe drug delivery systems. In another study, Sahoo et al. reported that biocompatible mesoporous silica nanoparticles coated with superparamagnetic manganese ferrite, selected for DOX delivery, did not cause DNA cleavage alone [66]. Moreover, the effects of green synthesized Ag nanoparticles on the bacterial DNA damage were more than those samples treated by chemically synthesized nanoparticles due to the presence of some phytochemical compounds on the surface of green ones [67].

Functionalized MSNs exhibited significantly lower hemolytic activity compared to free silver nanoparticles. Hemolysis activity decreased when AgNPs were attached to the surface of MSN-APTES. Furthermore, DOX loaded on MSN-AgNPs displayed less hemolytic activity than free DOX. These results indicated that MSNs-AgNPs can deliver DOX with a low hemolysis rate. Slowing et al. described the effects of MSNs on mammalian red blood cells (RBCs) and suggested that the hemolysis activity of MSNs is based on the interaction between the silanol groups on the surface of MSNs and the tetra alkyl ammonium groups on the membrane of RBCs. In addition, Solid-state NMR demonstrated that the silanol groups on MSNs contribute to their high biocompatibility and potential for diverse biological and medical applications [68]. Lin et al.

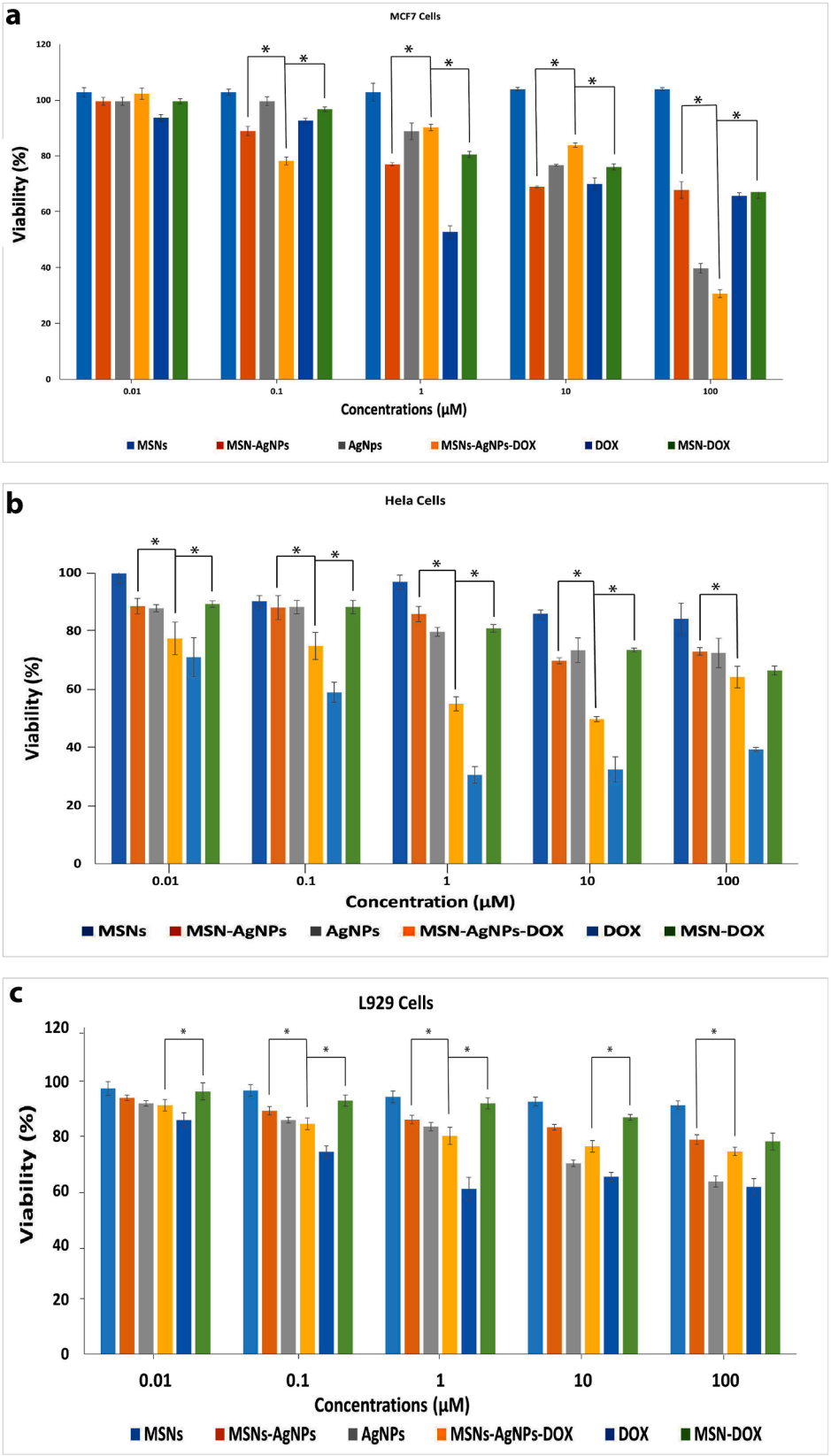


**Fig. 9.** Cytotoxicity assay of free DOX, MSNs, MSN-AgNPs, AgNPs, and MSN-AgNPs-DOX for different DOX concentrations (100 μM–0.01 μM) using a) MCF-7 cancer cells, b) Hela cancer cells and c) L929 cells. The asterisk represents significant differences in mean values for each parameter using Duncan's test (* $P < 0.05$).

**Table 4**
IC50 and Combination Index (CI) Values for MSN-AgNPs-DOX Formulation.

| Cell Line | IC50 of MSN-AgNPs-DOX (μM) | IC50 of MSN-DOX (μM) | IC50 of MSN-AgNPs (μM) | Combination Index (CI) |
|---|---|---|---|---|
| MCF-7 | 67.42 | 240.6 | 392.3 | 0.451 |
| HeLa | 10.0 | 235.8 | 20.7 | 0.522 |

corroborated this study using iron oxide nanoparticles attached to the mesoporous silica nanoparticles [69]. In some studies, it has been confirmed that when the drugs are loaded into mesoporous silica nanoparticles, hemolysis effects are reduced [70–72].

The cytotoxicity effects of MSNs, MSN-AgNPs, AgNPs, MSNs-AgNPs-DOX, and DOX were assessed on MCF-7 and Hela cells, providing insights into their potential for cancer treatment. Our results demonstrated that MSNs-APTES-AgNPs, at a concentration of 100 μM, induced the most significant rate of MCF-7 cell death, displaying a pronounced impact on cell viability, growth, and proliferation. This effect was more notable compared to nanoparticles without DOX and free DOX. In addition, DOX-loaded MSNs-AgNPs, at a concentration of 10 μM, were observed to induce death in half of the Hela cells.

Importantly, we noted the differential effect of MSNs-AgNPs-DOX formulation in tumoral versus non-tumoral cell lines. Specifically, in L929 mouse fibroblasts, the cytotoxic effect of the nanoformulation was notably reduced compared to MCF-7 cells, where their viability was strongly affected. This differential response suggests that our nanoformulation may have a preferential action against cancer cells, which is an invaluable characteristic for any chemotherapeutic agent, as it may contribute to reduced side effects on normal cells. Additionally, the results suggest the presence of a synergistic effect when MSNs-AgNPs and DOX are combined, potentially leading to a more effective treatment. Evaluating the combination index (CI) quantified this synergistic effect for both cell lines. In contrast, for L929 cells, there was no evident combination effect, which is favorable as it suggests reduced cytotoxicity on non-tumoral cells. This synergistic effect, which was selective for tumoral cells, further accentuates the potential advantages of using MSNs-AgNPs-DOX as a targeted delivery system for cancer treatment.

In addition, our finding suggested that DOX-loaded MSNs-AgNPs not only increased cell death in MCF-7 and Hela cells but also preserved the pharmaceutical activities of DOX. This observation may be attributed to the presence of positively charged MSN-APTES-AgNPs, which enhanced the delivery of the drug to the negatively charged cell membrane [42]. Our findings align with other investigations in the field. For instance, Chen et al. (2010), reported that DOX-loaded Fe3O4@mSiO2 nanocapsules displayed a substantial cytotoxic effect, which they attributed to the enhanced cellular uptake and accumulation of DOX loaded in the nanoparticles [73]. Li et al. (2022) designed photothermal-temperature responsive [Ag nanoparticles-hollow mesoporous silica nanospheres–poly (N-isopropyl acrylamide-acrylic acid)] (Ag@HMSN@P-NIPAM-AA) nanoparticles and investigated the combination of Ag nanoparticles (AgNPs) and [poly (N-isopropyl acrylamide-acrylic acid)] (PNIPAM-AA) for use as a switch of the photothermal-temperature effect to control drug release. Furthermore, they loaded DOX to the structure and indicated it had high human hepatoma cell inhibition under 808 nm near-infrared light [74]. The consistency of these findings highlights the potential of nanocarrier systems in improving the delivery and efficacy of chemotherapeutic agents like DOX. Therefore, by exploiting the advantages of nanotechnology, we can potentially improve the targeted delivery of chemotherapeutic agents, which could lead to increased efficacy and decreased side effects. However, further research is required to optimize these nanocarrier systems and to explore their potential in a broader array of cancer types.

## 5. Conclusions

In conclusion, our work successfully employed a green synthesis approach to develop AgNPs on the surface of amine-functionalized MSNs. The resulting nanoparticles are characterized by their nanoscale size and uniform morphology. To optimize the green synthesis of AgNPs, we identify the calyx extract, recognized for its potent antioxidant and anticancer proprieties, as an ideal candidate. Subsequent addition of this extract to the MSN-APTES suspension, post silver ion introduction, led to the creation of MSNs-AgNPs.

The drug loading and release studies revealed a high loading efficiency of the chemotherapeutic drug DOX onto the MSNs-AgNPs and a gradual release profile, well-suited for the dynamic of the cancer microenvironment. Interestingly, the cell cytotoxicity assay demonstrated a substantial reduction in cancer cell proliferation when treated with DOX encapsulated in the MSNs-AgNPs. These observations are particularly evident as they point to a significant decrease in the viability of breast and cervical cancer cells. We also observed a differential effect of the MSN-AgNPs-DOX nanoformulation on tumoral versus non-tumoral cell lines, which suggests preferential action against cancer cells. Moreover, the potential synergy between DOX and AgNPs in the MSN-AgNPs-DOX formulation, specifically in tumoral cells, may offer an avenue for enhanced therapeutic efficiency.

Despite these promising results, further investigations are necessary. The applicability of this novel delivery system i*n vivo* model needs to be established to determine its effectiveness and safety profiles. The potential synergistic effects of DOX and AgNPs, particularly their combined therapeutic implications, warrant further exploration. In conclusion, our study highlighted the potential of leveraging the power of green synthesis and nanotechnology to counteract cancer diseases. This work presents a new and promising direction for the development of more effective, targeted, and less cytotoxic cancer therapies, opening the door to novel therapeutic opportunities in oncology.

## Ethical approval

Not Applicable.

## Funding

M.C is supported by grant RYC2021-031003I funded by MICIU/AEI/https://doi.org/10.13039/501100011033 and, by European Union NextGenerationEU/PRTR.

**Research involving humans and animals statement**
Not Applicable. This is not an in vivo study.
**Informed consent**
Not Applicable. This is an in vitro study.

## CRediT authorship contribution statement

**Melika Ghobadi:** Writing – review & editing, Writing – original draft, Visualization, Methodology, Investigation. **Saeideh Salehi:** Writing – review & editing, Methodology, Investigation. **Mohammad Taha Salmanifard Ardestani:** Writing – review & editing, Visualization, Methodology, Investigation. **Mohammad Mousavi-Khattat:** Writing – review & editing, Visualization, Methodology, Investigation, Data curation. **Zahra Shakeran:** Writing – review & editing, Visualization, Methodology, Investigation, Formal analysis, Data curation. **Arezoo Khosravi:** Writing – review & editing, Methodology. **Marco Cordani:** Writing – review & editing, Visualization, Supervision, Investigation, Formal analysis, Conceptualization. **Ali Zarrabi:** Writing – review & editing, Visualization, Supervision, Methodology, Investigation, Formal analysis, Conceptualization.

## Declaration of competing interest

The authors declare that they have no known competing financial interests or personal relationships that could have appeared to influence the work reported in this paper.

## Data availability

Data will be made available on request.

## Acknowledgements

We would like to acknowledge deep regards to the "SETUP" laboratory members at Isfahan Science and Technology Town (ISTT), Isfahan University of Technology, Isfahan, Iran, for the excellent performance in conducting project in the laboratory.

## References

[1] O.M.A. Kweik, M.A.A. Hamid, S.O. Sheqlieh, B.S. Abu-Nasser, S.S. Abu-Naser, Artificial neural network for lung cancer detection, Int. J. Academic Eng. Res. (IJAER) 4 (2020) 1–7.
[2] S. Senapati, A.K. Mahanta, S. Kumar, P. Maiti, Controlled drug delivery vehicles for cancer treatment and their performance, Signal Transduct. Target. Ther. 3 (2018) 1–19.
[3] A. Jain, P.G. Fournier, V. Mendoza-Lavaniegos, P. Sengar, F.M. Guerra-Olvera, E. Iñiguez, T.G. Kretzschmar, G.A. Hirata, P. Juárez, Functionalized rare earth-doped nanoparticles for breast cancer nanodiagnostic using fluorescence and CT imaging, J. Nanobiotechnol. 16 (2018) 1–18.
[4] M.A. Aredo, E.G. Sendo, J.T. Deressa, Knowledge of cervical cancer screening and associated factors among women attending maternal health services at Aira Hospital West Wollega, Ethiopia, SAGE Open Medicine 9 (2021) 1–7.
[5] S. Lei, R. Zheng, S. Zhang, S. Wang, R. Chen, K. Sun, H. Zeng, J. Zhou, W. Wei, Global patterns of breast cancer incidence and mortality: a population-based cancer registry data analysis from 2000 to 2020, Cancer Commun 41 (2021) 1183–1194.
[6] M. Arbyn, E. Weiderpass, L. Bruni, S. de Sanjosé, M. Saraiya, J. Ferlay, F. Bray, Estimates of incidence and mortality of cervical cancer in 2018: a worldwide analysis, Lancet Glob. Health 8 (2020) e191–e203.
[7] X. Yi, W. Zeng, C. Wang, Y. Chen, L. Zheng, X. Zhu, Y. Ke, X. He, Y. Kuang, Q. Huang, A step-by-step multiple stimuli-responsive metal-phenolic network prodrug nanoparticles for chemotherapy, Nano Res. 15 (2022) 1205–1212.
[8] D. Lombardo, M.A. Kiselev, M.T. Caccamo, Smart nanoparticles for drug delivery application: development of versatile nanocarrier platforms in biotechnology and nanomedicine, J. Nanomater. 2019 (2019) 3702518.
[9] S. Paroha, J. Verma, R.D. Dubey, R.P. Dewangan, N. Molugulu, R.A. Bapat, P. K. Sahoo, P. Kesharwani, Recent advances and prospects in gemcitabine drug delivery systems, Int. J. Pharm. 592 (2021) 120043.
[10] S. Feng, J. Lu, K. Wang, D. Di, Z. Shi, Q. Zhao, S. Wang, Advances in smart mesoporous carbon nanoplatforms for photothermal–enhanced synergistic cancer therapy, Chem. Eng. J. 435 (2022) 134886.
[11] M. Vallet-Regí, Our contributions to applications of mesoporous silica nanoparticles, Acta Biomater. 137 (2022) 44–52.
[12] Q. Xu, Y. Yang, J. Lu, Y. Lin, S. Feng, X. Luo, D. Di, S. Wang, Q. Zhao, Recent trends of mesoporous silica-based nanoplatforms for nanodynamic therapies, Coord. Chem. Rev. 469 (2022) 214687.
[13] K. Wang, J. Lu, J. Li, Y. Gao, Y. Mao, Q. Zhao, S. Wang, Current trends in smart mesoporous silica-based nanovehicles for photoactivated cancer therapy, J. Control. Release 339 (2021) 445–472.
[14] F. Du, H. Meng, K. Xu, Y. Xu, P. Luo, Y. Luo, W. Lu, J. Huang, S. Liu, J. Yu, CPT loaded nanoparticles based on beta-cyclodextrin-grafted poly (ethylene glycol)/poly (L-glutamic acid) diblock copolymer and their inclusion complexes with CPT, Colloids Surf. B Biointerfaces 113 (2014) 230–236.
[15] S. Kanugala, S. Jinka, N. Puvvada, R. Banerjee, C.G. Kumar, Phenazine-1-carboxamide functionalized mesoporous silica nanoparticles as antimicrobial coatings on silicone urethral catheters, Sci. Rep. 9 (2019) 1–16.
[16] A.L. Doadrio, A.J. Salinas, J.M. Sánchez-Montero, M. Vallet-Regi, Drug release from ordered mesoporous silicas, Curr. Pharm. Des. 21 (2015) 6213–6819.
[17] P.K. Lavrič, B. Tomšič, B. Simončič, M.M. Warmoeskerken, D. Jocic, Functionalization of cotton with poly-NiPAAm/chitosan microgel: Part II. stimuli-responsive liquid management properties, Cellul. 19 (2012) 273–287.
[18] P. Xu, J. Yao, Z. Li, M. Wang, L. Zhou, G. Zhong, Y. Zheng, N. Li, Z. Zhai, S. Yang, Therapeutic effect of doxorubicin-chlorin E6-loaded mesoporous silica nanoparticles combined with ultrasound on triple-negative breast cancer, Int. J. Nanomed. 15 (2020) 2659.
[19] X. Wang, L. Wang, S. Zong, R. Qiu, S. Liu, Use of multifunctional composite nanofibers for photothermalchemotherapy to treat cervical cancer in mice, Biomater. Sci. 7 (2019) 3846–3854.
[20] K.L. Kelly, E. Coronado, L.L. Zhao, G.C. Schatz, The optical properties of metal nanoparticles: the influence of size, shape, and dielectric environment, J. Phys. Chem. B 107 (2003) 668–677.
[21] Z. Khan, S.A. Al-Thabaiti, A.Y. Obaid, A. Al-Youbi, Preparation and characterization of silver nanoparticles by chemical reduction method, Colloids Surf. B Biointerfaces 82 (2011) 513–517.
[22] M. Raffi, A.K. Rumaiz, M. Hasan, S.I. Shah, Studies of the growth parameters for silver nanoparticle synthesis by inert gas condensation, J. Mater. Res. 22 (2007) 3378–3384.
[23] J.M. Ashraf, M.A. Ansari, H.M. Khan, M.A. Alzohairy, I. Choi, Green synthesis of silver nanoparticles and characterization of their inhibitory effects on AGEs formation using biophysical techniques, Sci. Rep. 6 (2016) 1–10.
[24] R.M. Slawson, M.I. Van Dyke, H. Lee, J.T. Trevors, Germanium and silver resistance, accumulation, and toxicity in microorganisms, Plasmid 27 (1992) 72–79.
[25] K.C. Bhainsa, S. D'souza, Extracellular biosynthesis of silver nanoparticles using the fungus Aspergillus fumigatus, Colloids Surf. B Biointerfaces 47 (2006) 160–164.
[26] M. Kowshik, S. Ashtaputre, S. Kharrazi, W. Vogel, J. Urban, S.K. Kulkarni, K. M. Paknikar, Extracellular synthesis of silver nanoparticles by a silver-tolerant yeast strain MKY3, Nanotechnology 14 (2002) 95.
[27] S. Sarkar, V. Kotteeswaran, Green synthesis of silver nanoparticles from aqueous leaf extract of Pomegranate (Punica granatum) and their anticancer activity on human cervical cancer cells, Adv. Nat. Sci. Nanosci. Nanotechnol. 9 (2018) 025014.
[28] M.H. Nisha, R. Tamileswari, S.S. Jesurani, S. Kanagesan, M. Hashim, S.C. P. Alexander, Green synthesis of silver nanoparticles from pomegranate (Punicagranatum) leaves and analysis of anti-bacterial activity, Int. J. Adv. Technol. Eng. Sci. 4 (2015) 1–8.
[29] B. Şahin, E. Demir, A. Aygün, H. Gündüz, F. Şen, Investigation of the effect of pomegranate extract and monodisperse silver nanoparticle combination on MCF-7 cell line, J. Biotechnol. 260 (2017) 79–83.
[30] B. Şahin, A. Aygün, H. Gündüz, K. Şahin, E. Demir, S. Akocak, F. Şen, Cytotoxic effects of platinum nanoparticles obtained from pomegranate extract by the green synthesis method on the MCF-7 cell line, Colloids Surf.B: Biointerfaces 163 (2018) 119–124.
[31] M. Alomari, R.J. Balasamy, D. Almohazey, V. Ravinayagam, M. Al Hamad, D. Ababneh, H. Bahmdan, A.-H. Alomari, Z. Mokadem, A. Elaissari, Nile red-poly (methyl methacrylate)/silica nanocomposite particles increase the sensitivity of cervical cancer cells to tamoxifen, Polymers 12 (2020) 1516.
[32] B. Liu, L. Han, J. Liu, S. Han, Z. Chen, L. Jiang, Co-delivery of paclitaxel and TOS-cisplatin via TAT-targeted solid lipid nanoparticles with synergistic antitumor activity against cervical cancer, Int. J. Nanomed. 12 (2017) 955.
[33] N.K. Garg, B. Singh, A. Jain, P. Nirbhavane, R. Sharma, R.K. Tyagi, V. Kushwah, S. Jain, O.P. Katare, Fucose decorated solid-lipid nanocarriers mediate efficient delivery of methotrexate in breast cancer therapeutics, Colloids Surf. B Biointerfaces 146 (2016) 114–126.
[34] A. Hamidu, A. Mokrish, R. Mansor, I.S.A. Razak, A. Danmaigoro, A.Z. Jaji, Z. A. Bakar, Modified methods of nanoparticles synthesis in pH-sensitive nano-carriers production for doxorubicin delivery on MCF-7 breast cancer cell line, Int. J. Nanomed. 14 (2019) 3615.
[35] R.S. Fernandes, J.O. Silva, H.A. Seabra, M.S. Oliveira, V.M. Carregal, J.M. Vilela, M.S. Andrade, D.M. Townsend, P.M. Colletti, E.A. Leite, α-Tocopherol succinate loaded nano-structed lipid carriers improves antitumor activity of doxorubicin in breast cancer models in vivo, Biomed. Pharmacother. 103 (2018) 1348–1354.
[36] Y.L. Franco, T.R. Vaidya, S. Ait-Oudhia, Anticancer and cardio-protective effects of liposomal doxorubicin in the treatment of breast cancer, Breast Cancer: Targets and Therapy 10 (2018) 131.
[37] S. Wang, X. Liu, S. Chen, Z. Liu, X. Zhang, X.-J. Liang, L. Li, Regulation of Ca2+ signaling for drug-resistant breast cancer therapy with mesoporous silica nanocapsule encapsulated doxorubicin/siRNA cocktail, ACS Nano 13 (2018) 274–283.
[38] Y. Zhang, Y. Li, Z. Gao, B. Ding, P. An, X. Zhang, B. Sun, B. Sun, Mesoporous silica-coated silver nanoframes as drug-delivery vehicles for chemo/starvation/metal ion multimodality therapy, Langmuir 36 (2020) 6345–6351.
[39] A. Latorre, A. Latorre, M. Castellanos, C. Rodriguez Diaz, A. Lazaro-Carrillo, T. Aguado, M. Lecea, S. Romero-Pérez, M. Calero, J.M. Sanchez-Puelles, Multifunctional albumin-stabilized gold nanoclusters for the reduction of cancer stem cells, Cancers 11 (2019) 969.
[40] L. Qiu, Y. Zhao, N. Cao, L. Cao, L. Sun, X. Zou, Silver nanoparticle-gated fluorescence porous silica nanospheres for glutathione-responsive drug delivery, Sens. Actuators B 234 (2016) 21–26.
[41] X. He, F. Chen, Z. Chang, K. Waqar, H. Hu, X. Zheng, Y. Wang, W.f. Dong, C. Yang, Silver mesoporous silica nanoparticles: fabrication to combination therapies for cancer and infection, Chem. Rec. 22 (2022) e202100287.
[42] Z. Shakeran, M. Keyhanfar, J. Varshosaz, D.S. Sutherland, Biodegradable nanocarriers based on chitosan-modified mesoporous silica nanoparticles for delivery of methotrexate for application in breast cancer treatment, Mater. Sci. Eng. C 118 (2021) 111526.
[43] M. Sypabekova, A. Hagemann, D. Rho, S. Kim, 3-aminopropyltriethoxysilane (APTES) deposition methods on oxide surfaces in solution and vapor phases for biosensing applications, Biosensors 13 (2022) 36.
[44] Y. Tian, J. Qi, W. Zhang, Q. Cai, X. Jiang, Facile, one-pot synthesis, and antibacterial activity of mesoporous silica nanoparticles decorated with well-dispersed silver nanoparticles, ACS Appl. Mater. Interfaces 6 (2014) 12038–12045.

[45] M. Tavira, M. Mousavi-Khattat, Z. Shakeran, A. Zarrabi, PCL/gelatin nanofibers embedded with doxorubicin-loaded mesoporous silica nanoparticles/silver nanoparticles as an antibacterial and anti-melanoma cancer, Int. J. Pharm. 642 (2023) 123162.
[46] M. Mousavi-Khattat, M. Keyhanfar, A. Razmjou, A comparative study of stability, antioxidant, DNA cleavage and antibacterial activities of green and chemically synthesized silver nanoparticles, Artif. Cells Nanomed. Biotechnol. 46 (2018) S1022–S1031.
[47] H. Meng, M. Xue, T. Xia, Z. Ji, D.Y. Tarn, J.I. Zink, A.E. Nel, Use of size and a copolymer design feature to improve the biodistribution and the enhanced permeability and retention effect of doxorubicin-loaded mesoporous silica nanoparticles in a murine xenograft tumor model, ACS Nano 5 (2011) 4131–4144.
[48] Q. Cai, Z.-S. Luo, W.-Q. Pang, Y.-W. Fan, X.-H. Chen, F.-Z. Cui, Dilute solution routes to various controllable morphologies of MCM-41 silica with a basic medium, Chem. Mater. 13 (2001) 258–263.
[49] A. Davoudi, A. Tarang, S.A. Aleyasin, A. Salehi, R. Seighalani, F. Tahmoressi, Evaluation of two DNA extraction methods from maternal plasma for using in non-invasive bovine fetus gender determination, Iranian J. Reproductive Medicine 10 (2012) 523.
[50] D. Hassan, A.T. Khalil, A.R. Solangi, A. El-Mallul, Z.K. Shinwari, M. Maaza, Physiochemical properties and novel biological applications of callistemon viminalis-mediated α-Cr2O3 nanoparticles, Appl. Organomet. Chem. 33 (2019) e5041.
[51] W. Lei, C. Sun, T. Jiang, Y. Gao, Y. Yang, Q. Zhao, S. Wang, Polydopamine-coated mesoporous silica nanoparticles for multi-responsive drug delivery and combined chemo-photothermal therapy, Mater. Sci. Eng. C 105 (2019) 110103.
[52] L. Ma, M. Kohli, A. Smith, Nanoparticles for combination drug therapy, ACS Nano 7 (2013) 9518–9525.
[53] E. Chu, A. Sartorelli. (2018) Cancer chemotherapy, Lange's Basic and Clinical Pharmacology. 948-976.
[54] H. Ghazal, A. Waqar, F. Yaseen, M. Shahid, M. Sultana, M. Tariq, M.K. Bashir, H. Tahseen, T. Raza, F. Ahmad, Role of nanoparticles in enhancing chemotherapy efficacy for cancer treatment, Next Mater. 28 (2024) 100128.
[55] Y. Fu, J. Li, M. Almasi, Pomegranate peel extract-mediated green synthesis of silver nanoparticles: evaluation of cytotoxicity antioxidant, and anti-esophageal cancer effects, ChemistrySelect 8 (2023) e202204841.
[56] M. Abdelrazik, H.H. Elkotaby, A. Yousef, A.F. El-Sayed, M. Khedr, Green synthesis of silver nanoparticles derived from lemon and pomegranate peel extracts to combat multidrug-resistant bacterial isolates, J. Genet. Eng. Biotechnol. 21 (2023) 97.
[57] A.M. Alsamman, M. Khedr, H.A. Kabary, M. El-Sehrawy, Elimination of pathogenic multidrug resistant isolates through different metal oxide nanoparticles synthesized from organic plant and microbial sources, Microb. Pathog. 178 (2023) 106055.
[58] A.H. Hashem, G.S. El-Sayyad, Antimicrobial and anticancer activities of biosynthesized bimetallic silver-zinc oxide nanoparticles (Ag-ZnO NPs) using pomegranate peel extract, Biomass Convers. Biorefin. (2023) 1–13.
[59] A.A. Khan, A.M. Alanazi, N. Alsaif, T.A. Wani, M.A. Bhat, Pomegranate peel induced biogenic synthesis of silver nanoparticles and their multifaceted potential against intracellular pathogen and cancer, Saudi J. Biological Sci. 28 (2021) 4191–4200.
[60] M.L. Jeune, J. Kumi-Diaka, J. Brown, Anticancer activities of pomegranate extracts and genistein in human breast cancer cells, J. Med. Food 8 (2005) 469–475.
[61] Z. Amri, F. Zaouay, H. Lazreg-Aref, H. Soltana, A. Mneri, M. Mars, M. Hammami, Phytochemical content, fatty acids composition and antioxidant potential of different pomegranate parts: comparison between edible and non edible varieties grown in Tunisia, Int. J. Biol. Macromol. 104 (2017) 274–280.
[62] Y. Sun, K. Ma, T. Kao, K.A. Spoth, H. Sai, D. Zhang, L.F. Kourkoutis, V. Elser, U. Wiesner, Formation pathways of mesoporous silica nanoparticles with dodecagonal tiling, Nat. Commun. 8 (2017) 1–10.
[63] J.O. Otalvaro, M. Avena, M. Brigante, Adsorption of organic pollutants by amine functionalized mesoporous silica in aqueous solution. Effects of pH, ionic strength and some consequences of APTES stability, J. Environ. Chem. Eng. 7 (2019) 103325.
[64] Y. Li, Y. Yan, J. Wang, L. Li, F. Tang, Preparation of silver nanoparticles decorated mesoporous silica nanorods with photothermal antibacterial property, Colloids Surf.A: Physicochemical and Eng. Aspects 648 (2022) 129242.
[65] Y. Tang, H. Hu, M.G. Zhang, J. Song, L. Nie, S. Wang, G. Niu, P. Huang, G. Lu, X. Chen, An aptamer-targeting photoresponsive drug delivery system using "off–on" graphene oxide wrapped mesoporous silica nanoparticles, Nanoscale 7 (2015) 6304–6310.
[66] B. Sahoo, K.S.P. Devi, S. Dutta, T.K. Maiti, P. Pramanik, D. Dhara, Biocompatible mesoporous silica-coated superparamagnetic manganese ferrite nanoparticles for targeted drug delivery and MR imaging applications, J. Colloid Interface Sci. 431 (2014) 31–41.
[67] M. Mousavi-Khattat, H. Nourbakhshan, S. Afrazeh, S.H. Aminorroaya, Z. Shakeran, Donkey dung–mediated synthesis of silver nanoparticles and evaluation of their antibacterial, antifungal, anticancer, and DNA cleavage activities, BioNanoScience 12 (2022) 877–889.
[68] I.I. Slowing, C.W. Wu, J.L. Vivero-Escoto, V.S.Y. Lin, Mesoporous silica nanoparticles for reducing hemolytic activity towards mammalian red blood cells, Small 5 (2009) 57–62.
[69] Y.-S. Lin, C.L. Haynes, Synthesis and characterization of biocompatible and size-tunable multifunctional porous silica nanoparticles, Chem. Mater. 21 (2009) 3979–3986.
[70] B. Nepal, J.K. Bhattarai, K.B. Dhami, M.R. Nichols, K.J. Stine, Effect of mesoporous silica nanoparticles loaded with α-tomatine on HepG2 cancer cells studied in vitro, J. Drug Delivery Sci. Technol. 79 (2023) 104033.
[71] V. Krishnan, G.D. Venkatasubbu, T. Kalaivani, Investigation of hemolysis and antibacterial analysis of curcumin-loaded mesoporous SiO2 nanoparticles, Appl. Nanosci. 13 (2023) 811–818.
[72] Y. Jin, Y. Lu, A. Sathiyaseelan, K. Saravanakumar, X. Zhang, M.-H. Wang, Characterization, cytotoxicity, and antibacterial activity of paeoniflorin-loaded mesoporous silica oxide nanoparticles, J. Drug Delivery Sci. Technol. 84 (2023) 104551.
[73] Y. Chen, H. Chen, D. Zeng, Y. Tian, F. Chen, J. Feng, J. Shi, Core/shell structured hollow mesoporous nanocapsules: a potential platform for simultaneous cell imaging and anticancer drug delivery, ACS Nano 4 (2010) 6001–6013.
[74] M. Li, Y.H. Huang, Y.P. Qin, B. Ren, H.Y. Song, Y.J. Qi, Photothermally triggered control of the drug delivery system using doxorubicin-loaded mesoporous silica for effective killing of human hepatoma cells, Adv. Mat. Res. 1173 (2022) 91–98.